19th National & 8th ISHMT-ASME
Heat and Mass Transfer Conference
January 3 - 5, 2008
JNTU Hyderabad, India

Paper No:

Review of State of the Art Technologies used to Improve Performance of Thermoelectric Devices

A. Bulusu
Interdisciplinary Program in Materials Science
Vanderbilt University
Nashville, TN 37221
anuradha.bulusu@vanderbilt.edu

D. G. Walker
Department of Mechanical Engineering
Vanderbilt University
Nashville, TN 37221
greg.walker@vanderbilt.edu

Thermoelectric devices have gained importance in recent years as viable solutions for applications such as spot cooling of electronic components, remote power generation in space stations and satellites etc. These solid state devices have long been known for their reliability rather than their efficiency as they contain no moving parts. Research in recent years has been focused towards developing both thermoelectric structures and materials that have high efficiency characterized by the quantity known as the figure of merit $ZT = S^2\sigma T/\kappa$ where S is the Seebeck coefficient, σ the electrical conductivity and κ the thermal conductivity. In general thermoelectric research is two-pronged with 1) experiments focused towards finding new materials and structures with enhanced thermoelectric performance and 2) analytical models that predict thermoelectric behavior to enable better design and optimization of materials and structures. In this paper we present a review of the theoretical models that were developed since thermoelectricity was first observed in 1821 by Seebeck and how these models have guided experimental materials search for improved thermoelectric devices. A new quantum model is also presented, which provides opportunities for optimization of nanostructured materials to enhance thermoelectric performance.

1. Thermoelectric properties

When two wires of different metals are joined at both ends and the two junctions are kept at different temperatures, a voltage develops across the two junctions. This effect is known as the Seebeck effect which was discovered by Seebeck in 1821 and published in 1822 [1]. The voltage across the two junctions is proportional to the temperature gradient across the junctions provided the temperature gradient is small. The proportionality constant is defined as the Seebeck coefficient or thermoelectric power and is obtained from the ratio of the voltage generated and the applied temperature gradient.

$$S = \frac{dV}{dT} \qquad (1)$$

In 1834, the Peltier effect was discovered [2]. When two metals are joined together and kept at constant temperature while a current passes across the junction, heat is generated or absorbed at that junction in addition to Joule heating. The Peltier coefficient Π_{12} is defined as the heat emitted per second when unit current flows from conductor 1 to 2. This heat is directly proportional to the current passing through the junction as described by equation 2.

$$dQ = \prod dI \qquad (2)$$

The Thomson effect was predicted in 1854 and found experimentally in 1856 [3]. The Thomson effect occurs when a current flows across two points of a homogeneous wire having a temperature gradient along its length and heat is emitted or absorbed in addition to the Joule heat. The Thomson coefficient μ_T is positive if heat is generated when positive current flows from a higher temperature to lower temperature.

$$dQ = \mu_T \frac{\partial T}{\partial x} dx dI \qquad (3)$$

These three thermal-electrical properties provide the basis for modern direct energy conversion devices and their exploitation is the subject of considerable research.

2. Nanostructured thermoelectric materials

The advent of quantum well nanofilm and nanowire superlattice structures that improve the value of *ZT* due

to a number of advantages has shifted the focus towards understanding carrier transport behavior in nanostructures. Quantum confinement in nanostructures increases the local carrier density of states per unit volume near the Fermi energy increasing the Seebeck coefficient [4] while the thermal conductivity can be decreased due to phonon confinement [5, 6] and phonon scattering at the material interfaces in the superlattices [4, 7, 8]. Normally, the electrical conductivity is assumed *not* to be significantly affected due to the large semiconductor bandgap and the disparity between the electron and phonon mean free paths [25, 9]. The combined benefits of reduced thermal conductivity and improved Seebeck coefficient imply a theoretically higher *ZT* compared to the bulk structures. However, experimental observations have not been able to achieve the presumed benefits of superlattice thermoelectric devices despite theoretically predicted improvements in *ZT* and experimentally observed reduction in the thermal conductivity of superlattices compared to their bulk counterparts [10, 11]. Hence there is a need to better understand the effect of all the significant factors contributing to the thermoelectric figure of merit of nanoscale devices. In this regard, the two main phenomena that affect electron transport in nanostructures are 1) electron confinement and 2) electron scattering effects such as electron-phonon scattering, electron-impurity scattering etc.

Shrinking device dimensions presents an increasing need for a quantum transport model that can effectively couple scattering effects. The need to incorporate scattering stems from the fact that while electron-phonon scattering usually helps restore thermodynamic equilibrium, shrinking device dimensions may not ensure enough scattering to restore equilibrium. The simultaneous consideration of scattering effects, which is usually described as particle behavior, and quantum effects, which are wave in nature, is confounding and computationally intensive. In this regard the non-equilibrium Green's function formalism provides a framework for coupling quantum effects and thermal effects to model electron transport in thermoelectric devices. Open boundary conditions allow the source and drain contacts to be coupled to the device through simple self-energy terms. In addition, the NEGF formalism *does not* require a statistical distribution of carriers within the device thus allowing for the rigorous incorporation of both elastic and inelastic scattering effects using the concept of Buttiker probes [12]. A brief synopsis of the formalism is presented here while a more thorough and detailed development can be found in [12] and [13]. The first reported use NEGF to predict thermoelectric performance is found in [14, 15]. True quantum simulations have to see widespread use, but modern devices demand this level of modeling.

3. The NEGF Formalism

In general an isolated device and its energy levels are described using a Hamiltonian H, a Hartree potential U and energy eigen-states of the electron, ε_α.

$$\left(H+U\right)\psi_\alpha\left(\vec{r}\right)=\varepsilon_\alpha\psi_\alpha\left(\vec{r}\right) \quad (4)$$

The potential U is obtained using Poisson's equation and accounts for the effect of any change in the density matrix on the channel capacitance. The channel capacitance consists of an electrostatic capacitance that depends on the dielectric constant ε_r and a quantum capacitance, which depends on the density of Eigen states in the channel [13]. In general, the electron density matrix in real space is given by

$$\left[\rho(\vec{r},\vec{r}';E)\right]=\int_{-\infty}^{+\infty} f\left(E-\mu\right)\delta\left(\left[EI-H\right]\right)dE \quad (5)$$

Here $\delta(EI\text{-}H)$ is the local electronic density of states given as

$$\delta\left(EI-H\right)=\frac{i}{2\pi}\left[G\left(E\right)-G^{+}\left(E\right)\right] \text{where}$$

$$G\left(E\right)=\left[\left(E-i0^{+}\right)I-H\right]^{-1} \quad (6)$$

G(E) is the retarded Green's function while $G^{+}(E)$, its conjugate complex transpose, is called the advanced Green's function. In the time domain, the Green's function can be interpreted as the impulse response of the Schrödinger equation where in the present scenario the impulse is essentially an incoming electron at a particular energy. In the energy domain the Green's function gives the energy eigen-values for the eigen-states that are occupied in response to the applied impulse. The diagonal elements of the spectral function, which is the difference between the retarded and advanced Green's function, represent the available local electron density of states.

When the isolated device is connected to source and drain contacts, the difference in the Fermi levels of the source and drain causes electrons to flow from the source to the drain through the channel. The distribution of electrons in the semi-infinite source and drain is said to follow the Fermi distribution with ε_{f1} and ε_{f2} the chemical potentials of the source and the drain and f_1 and f_2 their Fermi functions. When no scattering is incorporated in the channel, transport is ballistic in nature and is expected to have zero resistance to current flow. However, experimental measurements [16] have shown that the maximum measured conductance of a *one-energy* level channel approaches a limiting value $G_0 = 2q^2/\hbar$ = 51.6(KΩ)-1. The reason for this limit to conductance arises from the fact that current in the contacts is carried by infinite transverse modes while the number of available modes for a one-energy level channel is very limited. When the channel consisting of a single energy level ε is connected to the contacts current can flow only when ε lies between ε_{f1} and ε_{f2} ($\varepsilon_{f1} > \varepsilon > \varepsilon_{f2}$). Once the value of

ε is ensured to lie near ε_{f1} some of the density of states from the source spread into the channel causing broadening of the available density of states around ε (refer to Figure 1). There will be some broadening of energy levels around the drain as well but if the difference between ε and ε_{f2} is large, the broadening will be very small and only few states will become available near the drain to remove the electrons coming from the channel. As the applied bias is increased linearly, more and more states between ε and ε_{f2} become available to remove electrons from the channel causing the source to increase its supply of electrons into the channel. This phenomenon results in a linear increase of current in the channel. Once the applied bias causes the source and drain Fermi levels to become equal, the number of available density of states remains constant at the energy level ε and the channel current reaches saturation and the current will not increase any further. The above analogy of a one-energy level system is applicable to nanoscale thin films and wires where available energy levels along the confined dimension are very limited in addition to being spaced far apart from adjacent energy levels.

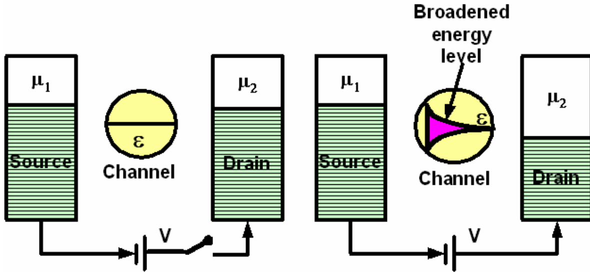

Figure 1. (a) Single energy level of an isolated channel (b) Broadening of electron energy levels in the channel when connected to contacts

In the NEGF formalism the coupling of the device to the source and drain contacts is described using self-energy matrices Σ_1 and Σ_2. The self-energy term can be viewed as a modification to the Hamiltonian to incorporate the boundary conditions. Accordingly, equation 4 can be rewritten as

$$\left(H+U+\Sigma_1+\Sigma_2\right)\psi_\alpha\left(\vec{r}\right)=\varepsilon_\alpha\psi_\alpha\left(\vec{r}\right) \quad (7)$$

The self-energy terms Σ_1 and Σ_2 originate from the solution of the contact Hamiltonian. In this semi-infinite system, which is connected to the channel, there will be an incident wave from the channel as well as a reflected wave from the contact. The wave function at the interface is matched to conserve energy resulting in the boundary condition,

$$\Sigma_j=-t\exp\left(ik_ja\right) \quad (8)$$

where t, the inter-unit coupling energy resulting from the discretization is given by

$$t=\frac{\hbar^2}{2m^*a^2}. \quad (9)$$

The broadening of the energy levels introduced by connecting the device to the source and drain contacts is incorporated through the Gamma functions at each contact given by

$$\Gamma_j=i\left(\Sigma_j-\Sigma_j^+\right) \quad (10)$$

The self-energy terms affect the Hamiltonian in two ways. The real part of the self-energy term shifts the device eigenstates or energy level while the imaginary part of Σ causes the density of states to broaden while giving the eigenstates a finite lifetime. The electron density for the open system is now given by

$$\left[\rho\right]=\int_{-\infty}^{+\infty}\left[G(E)\Sigma^{in}(E)G^+(E)\right]\left(\frac{dE}{2\pi}\right) \quad (11)$$

$$\text{where } \left[\Sigma^{in}(E)\right]=\left[\Gamma_1(E)\right]f_1+\left[\Gamma_2(E)\right]f_2 \quad (12)$$

The real portion of the diagonal elements of the density matrix, represent the electron density distribution in the channel. This electron density represented as n is used in the Poisson's equation to self-consistently solve for the potential in the channel where N_d is the donor density and ε_r is the permittivity of the channel.

$$\nabla^2U=-\frac{q}{\varepsilon_r}\left(N_d-n\right) \quad (13)$$

For plane wave basis functions, the current through the channel is calculated as the difference between the inflow and the outflow at any given contact.

$$I_j=-\frac{q}{\hbar}\int_{-\infty}^{\infty}trace\left[\Gamma_jA\right]f_j-trace\left[\Gamma_jG^n\right] \quad (14)$$

where the subscript j indexes the contacts. For a two-terminal device $I_1=-I_2$.

3.1. Incorporating electron scattering in the NEGF

In addition to the source and drain contacts electrons can scatter into and out of the channel by either phonon absorption or phonon emission such that ε_n - ε_m = □ω. The transition of the electrons from ε_n to ε_m and vice versa is dependent on the transition rate *S(k, k')* which is obtained using Fermi's Golden Rule [17]. This coupling can be expressed through a broadening term Γ which is related to the transition rate S as

$$\frac{\Gamma}{\hbar} = S(k,k') \quad \text{where}$$

$$\Gamma_{nn} = 2\pi\left|K_{mn}^{em}\right|^2 (N+1)\delta(\varepsilon_n - \varepsilon_m - \hbar\omega)$$
$$+2\pi\left|K_{mn}^{ab}\right|^2 (N)\delta(\varepsilon_n - \varepsilon_m + \hbar\omega)$$
(15)

The broadening term obtained through Fermi's Golden Rule is similar to the broadening term in the NEGF which is expressed as

$$\Gamma_s = \int \frac{d(\hbar\omega)}{2\pi}\left[\begin{array}{l} S_o^{em}(N_\omega+1)\left[G^p(E-\hbar\omega)+G^n(E+\hbar\omega)\right]+ \\ S_o^{ab}(N_\omega)\left[G^n(E-\hbar\omega)+G^p(E+\hbar\omega)\right] \end{array}\right]$$
(16)

$G^n(E)$ is the electronic density of states and $G^p(E)$ is the hole density of states and correspond to the $\delta(\varepsilon_n - \varepsilon_m \pm \hbar\omega)$ terms while S_o corresponds to the value $|K_{mn}|^2$ terms for emission and absorption of phonons in equation 16. For the case where electrons in the channel scatter with a phonon of single frequency, the broadening term can be simplified to

$$\Gamma_s = S_o\left[\begin{array}{l} (N_\omega+1)\left[G^p(E-\hbar\omega)+G^n(E+\hbar\omega)\right]+ \\ N_\omega\left[G^n(E-\hbar\omega)+G^p(E+\hbar\omega)\right] \end{array}\right]$$
(17)

Since the imaginary part of the self energy term is responsible for broadening, the scattering self-energy Σ_s can be expressed using equation 17 as

$$\Sigma_s = -i\frac{\Gamma_s}{2} \qquad (18)$$

The value of S_o for a single phonon of energy □ω_o is obtained as a sum over all phonon wave vectors β in the Brillouin zone as

$$S_o = \sum_\beta \frac{D_o^2\hbar^2}{2\rho\Omega(\hbar\omega_o)} = \frac{D_o^2\hbar^2}{12\pi^2\rho(\hbar\omega_o)}\left(\frac{\pi}{a}\right)^3$$
(19)

ρ is the mass density, ω_o the phonon frequency and D_o is the optical deformation potential and a, the lattice constant. An example of single-phonon scattering is g-type intervalley longitudinal optical-phonon scattering of electrons from the [001] valley into the [00♣] valley in silicon [17]. The scattering self energy is included in the Green's function seen in equation 20 as an additional contact that scatters electrons into and out of the channel such that the net current through the scattering contact is zero.

$$G(E) = \left[(E - i0^+)I - H - \Sigma_1 - \Sigma_2 - \Sigma_s\right]^{-1}$$
(20)

4. Results

The NEGF method is used to calculate the current density for varying thickness of a silicon film for a constant applied field of 10^6 V/m as shown in figure 2. The current density is obtained for two cases 1) ballistic electron transport through the film and 2) electrons undergoing intervalley scattering with longitudinal optical phonons. The electrons in a 2D film can be treated as having infinite range of energies along the x and y axis while being confined along the z-axis which is also the direction of transport.

$$E(k) = E_c + \frac{\hbar^2 k_x^2}{2m_x^*} + \frac{\hbar^2 k_y^2}{2m_y^*} + \frac{\hbar^2}{2m_z^*}\left(\frac{n\pi}{L_z}\right)^2$$
where n = 1, 2, 3……(21)

Two important effects are demonstrated in figure 2. The current is very small for small film thicknesses and increases as the film thickness increases. This is the effect of electron confinement where the very small film leads to discrete subband energies that are spaced far apart in the energy space of the Brillouin zone. The electrons in thin films have very limited number of subbands available for transport leading to low current density. The second important effect is the impact of longitudinal electron-phonon scattering on the current density. Since very small films have limited states available for electron transport, electrons cannot easily scatter into or out of the subbands spaced far apart from each other. As a result, the effect of scattering is very small for film thicknesses up to 5nm. As the film thickness increases, the subband energies are spaced closer to each other and are also lower in energy as they come closer to the conduction band edge. As a result the effect of scattering begins to gain significance for film thicknesses greater than 5nm where the decrease in current is now 10% of the ballistic current.

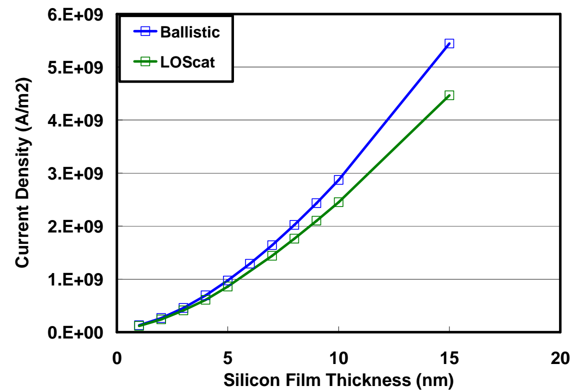

Figure 2. Current density vs. thickness of silicon film doped to $10^{18}cm^{-3}$ for (a) ballistic electron transport and (b) electron transport with longitudinal optical-phonon scattering.

The NEGF is used to calculate the Seebeck coefficient, electrical conductivity and power factor of silicon 6nm and 12nm films and 6nm x 6nm wire. The Seebeck

coefficient for the silicon film and wire was calculated by applying a temperature gradient along the z-axis. This was achieved by keeping the source temperature constant at 300K while changing the drain temperature in increments of 10K from 300K to 330K. The applied bias ranged from 0 to 0.05V. At low bias conditions, the higher temperature at the drain results in diffusion of electrons from the drain towards the source, opposing the direction of the bias leading to negative current values. As the applied bias is increased, more electrons from the source drift towards the drain and at a particular voltage, which we call the Seebeck voltage; the diffusion of electrons from the drain to the source is balanced by the drift current from the source to the drain leading to zero current. The Seebeck voltage obtained for each temperature gradient is divided by that value of the gradient to obtain the Seebeck coefficient. The current-voltage characteristics were calculated for the conduction band and 2 contributing subbands in the case of the 6nm film and 6 subbands in the case of the 12nm film.

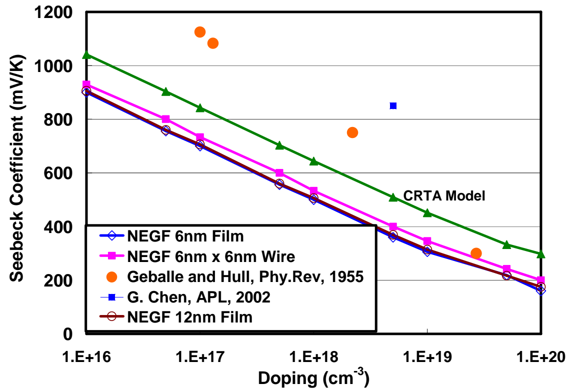

Figure 3. Seebeck coefficient of silicon films and wires calculated using NEGF and one-subband RTA model [4] compared to experiments [17, 18].

Figure 3 shows the predicted and measured Seebeck coefficient values for silicon 2D film and 1D wire for various doping levels in all temperature ranges considered. The effect of confinement is more evident from the 2D film to the 1D wire as seen from the increase in the Seebeck coefficient of the wire by approximately 30μV/K compared to the film for the same doping level. The effect of increase in the local density of states per unit volume near the Fermi energy is greater in the wire compared to the film. As a result, more carriers occupy higher energy states causing an increase in the value of the voltage for which the thermally induced current is balanced by the field current. The experimental values for the Seebeck coefficient were measured for a wide range of temperatures while the values used here are an average for the temperature range of 300K to 330K. While there is limited experimental data for the Seebeck coefficient of silicon nanofilms, the predicted values of S for the film match the experimental trends [17]. The NEGF results are also compared to the Seebeck coefficient predicted using the RTA model for a single band in 6nm film having a confined dispersion. We do not expect an exact match due to the very different nature of the two models. However, the Seebeck coefficient values from the NEGF model follow a similar trend as the RTA model.

Figure 4 shows the electrical conductivity values as a function of doping for 6nm silicon film obtained from the NEGF and RTA models for a single subband. Doping in both models is applied using equation 22 by varying the relative difference between the Fermi level and conduction band edge [19].

$$n = N_c \exp\left(-\frac{\left(E_c - E_f\right)}{k_B T}\right) \qquad (22)$$

In addition, the RTA model requires the value of mobility in the direction of transport for electrical conductivity calculations. Because of the conflict in the electron mobility behavior with decreasing film thickness seen in the literature [20, 21, 22, 23], we use the bulk mobility value of silicon as a benchmark for calculating the electrical conductivity using the RTA model. The conductivity values predicted by the RTA model for a single subband are almost equal to the NEGF method for the 6nm film summed over the conduction band and 2 subbands. This result implies that the RTA model over predicts the electrical conductivity. The 2 subbands for the NEGF model were chosen based on the proximity of the subband energy levels to the conduction band. If a similar analysis is applied for the RTA model, we will need to sum over an additional subband that will in turn increase the predicted conductivity. These results support our hypothesis that confinement effects dominate at these size regimes and are effectively captured by the NEGF model.

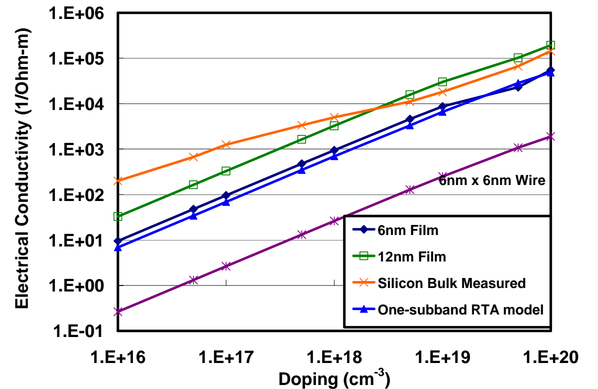

Figure 4. Predicted and measured [24] electrical conductivity values for a Silicon 6nm and 12nm film and 6nmx6nm wire.

Confinement of electrons increases the spacing between adjacent subband energy levels leading to a linear increase in the electrical conductivity with size. For example, a 12nm film can accommodate twice the number of electronic energy levels compared to a 6nm film and hence the conductivity of a 12nm film is twice the conductivity of a 6nm film. In reality and as seen from figure 2, as the size of the film increases,

transport is no longer ballistic and the conductivity is expected to reach a maximum before starting to reduce with increase in size due to the dominance of scattering. This effect is evident in figure 5 from the plot of the power factor of a 6nm silicon film with intervalley optical phonon scattering included in the NEGF formalism. Despite the 6nm film exhibiting very low scattering of approximately 10% for a doping of $10^{18}cm^{-3}$ as seen in figure 2, at large doping the number of carriers available to scatter is higher leading to 20% decrease in the power factor for a doping of $10^{19}cm^{-3}$ and a further decrease of 45% for $5x10^{19}cm^{-3}$ doping. The decrease in power factor is dominated by the decrease in electrical conductivity though scattering causes a slight (30μV/K) decrease in the Seebeck coefficient.

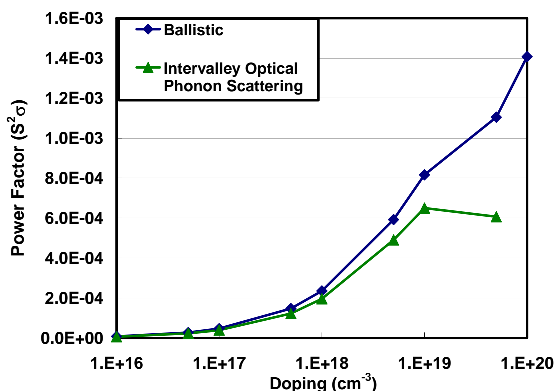

Figure 5. Power factor of a 6nm film with and without intervalley scattering predicted using the NEGF formalism.

5. Conclusion

We present a review of the state of the art for modeling techniques used to predict the performance of thermoelectric devices. Models based on Boltzmann and Fermi-Dirac statistics coupled in semi-classical transport have been very effective in identifying the pertinent physical parameters responsible for thermoelectric performance in bulk materials. In addition, the inclusion of various scattering mechanisms through the relaxation time approach allow us to isolate and understand carrier scattering mechanisms that dominate thermoelectric performance for a particular temperature range. While the semi-classical models work well in predicting the performance of materials in the bulk regime, wave effects that can not be captured naturally in particle-based models begin to dominate in nanostructured materials. Reduced dimensionality results in phonon confinement and formation of phonon bandgaps as well as tunnelling and diffraction of electrons, characteristic of wave behavior. Furthermore, alteration of the dispersion relations of electrons and phonons at nanoscales affects the way these carriers interact with each other.

A quantum transport model that can successfully couple wave effects and scattering effects to predict thermoelectric performance is introduced through the non-equilibrium Green's function method. In addition to successfully coupling quantum and scattering effects, the NEGF method allows us to seamlessly include various parameters that affect thermoelectric performance such as bandgaps, doping, and effective mass. The coupled thermoelectric solution combined with quantum effects demonstrates the capability of the NEGF method as a platform to design structures with enhanced figure of merit. In addition to studying thermoelectric transport at nanoscales, the NEGF method will also act as a framework for analysis of other emerging technologies in the field of solid-state energy conversion devices where temperature effects on carrier transport are strong.

Reliance on Boltzmann-based models has produced a culture of ``smaller is better'' research, where the reduction in size is expected to produce limitless increases in performance. Experiments have not exhibited this behavior, and with a combined wave/particle model we have been able to explain the apparent discrepancy. For materials at reduced scales, the governing physics changes enough that new models are required. The NEGF model suggests that optimization of devices is possible. Although this places theoretical upper limits on performance, there is no indication that these theoretical limits have been reached and continued research is warranted.

6. References

[1] T. J. Seebeck, The magnetic polarization of metals and ores produced by temperature difference, Proc. of Prussian Acad. of Sciences, 265-373.
[2] J. C. Peltier, Nouvelles experiences sur la caloriecete des courans electriques, Ann. of Chem., LVI, 371-387, 1834.
[3] W. Thomson, On a mechanical theory of thermoelectric currents, Proc. Roy. Soc. of Edinburgh, 91-98, 1851.
[4] L. D. Hicks and M. S. Dresselhaus, Effect of quantum-well structures on the thermoelectric figure of merit, Phy. Rev. B, 47, 19, 12727-12731, 1993.
[5] A. Balandin, and K. L. Wang, Significant decrease of the lattice thermal conductivity due to phonon confinement in a free-standing semiconductor quantum well, Phy. Rev. B, 58, 3, 1544-1549, 1998.
[6] A. Balandin and K. L. Wang, Effect of phonon confinement on the thermoelectric figure of merit of quantum wells, J. of Appl. Phy., 84, 11, 6149-6153, 1998.
[7] L. D. Hicks, T. C. Harman and M. S. Dresselhaus, Use of quantum-well superlattices to obtain a high figure of merit from non-conventional thermoelectric materials, Appl. Phy. Let., 63, 23, 3230-3232, 1993.
[8] L. W. Whitlow and T. Hirano, Superlattice applications to thermoelectricity, J. of Appl. Phy., 78, 9, 5460-5466, 1995.

[9] M. S. Dresselhaus, Nanostructures and energy conversion, Proc. of 2003 Rohsenhow Symposium on Future Trends of Heat Transfer, Cambridge, MA, May 16.
[10] T. Koga, S. B. Cronin, M. S. Dresselhaus, J. L. Liu and K. L. Wang, Experimental proof-of-principle Investigation of enhanced $Z_{3D}T$ in 001 oriented Si/Ge superlattices, Appl. Phy. Let., 77, 10, 1-3, 2000.
[11] T. M. Tritt, 2001, Recent Trends in Thermoelectric Materials Research, Vol. III, Semiconductors and Semimetals, 69, 70, 71.
[12] S. Datta, Nanoscale Device Simulation: The Green's function formalism, Superlattices and Microstructures, 28, 253-278, 2000.
[13] S. Datta, Quantum Transport: Atom to Transistor, New York: Cambridge University Press, 2005.
[14] A. Bulusu and D. G. Walker, Modeling of thermoelectric properties of semiconductor thin films with quantum and scattering effects, J. of Heat Transfer, 129, 2007.
[15] A. Bulusu and D. G. Walker, Quantum modeling of thermoelectric Properties of Si/Ge/Si superlattice, submitted to IEE Trans. Of Elect. Dev., 2007.
[16] A. Szafer and A. D. Stone, Theory of quantum conduction through a constriction, Phys. Rev. Let., 62, 300-303, 1989.
[17] M. Lundstrom, Fundamentals of Carrier Transport, Cambridge University press, 2000.
[18] T. H. Geballe and G. W. Hull, Seebeck effect in silicon, Phys. Rev., 98, 4, 940-947, 1955.
[19] R. Muller, T. Kamins and M. Chan, Device Electronics for Integrated Circuits, Wiley, New York, 1986.
[20] J. H. Choi, Y. J. Park and H. S. Min, Electron mobility behavior in extremely thin SOI MOSFETs," IEEE Elect. Dev. Let, 16, 11, 527-529, 1995.
[21] S. Takagi, J. Koga and A. Toriumi, Subband structure engineering for performance enhancement of Si MOSFETs," IEEE Trans. of IEDM, 219-222, 1997.
[22] T. Wang, T. H. Hsieh and T. W. Chen, Quantum confinement effects on low-dimensional electron mobility, J. of Appl. Phy., 74, 1, 426-430, 1993.
[23] V. A. Fonoberov and A. A. Balandin, Giant enhancement of the carrier mobility in silicon nanowires with diamond coating, Nano Letters, 6, 11, 2442-2446, 2006.
[24] S. M. Sze, Physics of Semiconductor Devices, Wiley-Interscience, 1969.
[25] H. Bottner, G. Chen and R. Venkatasubramanian, "Aspects of thin-film superlattice thermoelectric materials, devices and applications," Mat. Res. Sc. Bulletin, **31**, 211-217, March 2006.